



## Variation in shortwave water vapour continuum and impact on clear-sky shortwave radiative feedback.

Kaah P. Menang<sup>1,2</sup>, Stefan A. Buehler<sup>2</sup>, Lukas Kluft<sup>3</sup>, Robin J. Hogan<sup>4</sup> and Florian E. Roemer<sup>2</sup>

1. Department of Physics, University of Buea, Cameroon

5 2. Meteorological Institute, Department of Earth Sciences, Faculty of Mathematics, Informatics and Natural Sciences, University of Hamburg, Hamburg, Germany

3. Max Planck Institute for Meteorology, Hamburg, Germany

4. European Centre for Medium-Range Weather Forecasts, Reading, UK

10 *Correspondence to:* Kaah P. Menang (kaah.menang@ubuea.cm)

**Abstract.** This work assesses the impact of the current differences in the strength of the shortwave water vapour continuum on clear-sky calculations of shortwave radiative feedback. Four continuum models were used: the MT\_CKD (Mlawer-Tobin-Clough-Kneizys-Davies;  
15 versions 2.5, 3.2 and 4.1.1) and CAVIAR (Continuum Absorption at Visible and Infrared Wavelengths and its Atmospheric Relevance) models. Radiative transfer calculations were performed with the ECMWF radiation scheme ('ecRad'). The correlated  $k$ -distribution gas-optics tables required for ecRad computations were trained with each of these continuum models using the ECMWF software tool. The gas-optics tables trained with the different  
20 continuum models were used alternatively in the shortwave. The atmosphere configuration was; fixed surface temperatures ( $T_s$ ) between 270–330K, fixed relative humidity at 80%, a moist adiabatic lapse rate for the tropospheric temperature and an isothermal stratosphere with the tropopause temperature fixed at 175K. At  $T_s=288$ K, it was found that the revisions of the MT\_CKD model in the shortwave over the last decade have a modest effect ( $\sim 0.3\%$ ) on the  
25 estimated shortwave feedback. Compared to MT\_CKD 4.1.1, the stronger CAVIAR model has a relatively greater impact; the shortwave feedback is  $\sim 0.006 \text{ Wm}^{-2} \text{ K}^{-1}$  ( $\sim 1.6\%$ ) more positive. The uncertainty in the shortwave feedback increases up to  $0.008 \text{ Wm}^{-2} \text{ K}^{-1}$  ( $\sim 2.0\%$ ) between the MT\_CKD models and  $0.018 \text{ Wm}^{-2} \text{ K}^{-1}$  ( $\sim 4.6\%$ ) between CAVIAR and MT\_CKD 4.1.1 models at  $T_s \approx 300$ K. Constraining the shortwave continuum will contribute to reducing the non-  
30 negligible shortwave feedback uncertainties at higher  $T_s$ .



## 35 1. Introduction

The concept of radiative-convective equilibrium (RCE), in which there is an energy balance between radiative cooling of the atmosphere and convective heating, is the simplest possible description of the climate system. Observations show that this idealisation of the climate system is a fairly accurate simplification of the tropical atmosphere (e.g., Popke et al., 2013; Kluft et al., 2019). Thus, different hierarchies of RCE atmospheric models have been used to study the Earth's tropical climate over the years (see, for example, Becker and Wing, 2020 and references therein). In particular, RCE models have in the last decade been used to investigate, equilibrium climate sensitivity (ECS), radiative feedbacks, precipitation extremes and equilibrium climate as well the factors that influence them (e.g., Popke et al., 2013; Meraner et al., 2013; Reed et al., 2015; Dacie et al., 2019; Kluft et al., 2019; Becker and Wing, 2020; Wing et al., 2020).

Despite having the fewest number of interactive processes within the RCE model hierarchy, the one-dimensional (1D) RCE model is fundamental in obtaining the first estimates of radiative feedbacks and ECS, which are important for understanding climate and climate change of the tropics (e.g., Ramanathan and Coakley, 1978). For example, Manabe and Wetherald (1967) used a 1D RCE model to robustly estimate the ECS and water vapour feedback that have stood the test of time. However, there have been significant disagreements over the values of these (and other) quantities calculated from 1D RCE models (e.g., Schlesinger, 1986; Kluft et al., 2019). Factors that may lead to uncertainties in 1D RCE calculations of these climate parameters include; vertical relative humidity (RH) distribution, concentration of atmospheric gases, clouds and radiative transfer calculations. Recently, Bourdin et al. (2021) and Kluft et al. (2019) have shown that differences in the vertical distribution of RH have a significant impact on 1D RCE clear-sky calculations of radiative feedbacks and ECS. In another study, Dacie et al. (2019) concludes that 1D RCE clear-sky calculations of the tropical tropopause layer and surface climate are sensitive to CO<sub>2</sub> concentration and ozone profile. Kluft (2020) showed that the presence of clouds has a significant impact on 1D RCE calculations of radiative feedbacks and forcings. Kluft et al. (2019) speculated that the differences in the treatment of radiative transfer may be an additional reason for some discrepancies in estimated climate quantities, such as ECS, by different 1D RCE studies. But they did not specify the aspect (s) of radiative transfer that could contribute to these uncertainties.



The atmospheric absorption by water vapour is an essential aspect of radiative transfer calculations in 1D RCE (and other climate) models (e.g., Kratz, 2008). Unlike the water vapour spectral-line absorption which is well-understood, absorption by the water vapour continuum is still uncertain, with larger uncertainties in atmospheric windows at shorter wavelengths (e.g., Shine et al., 2016). The uncertainties in the water vapour continuum absorption have contributed to discrepancies in the estimation of the shortwave absorption from climate models, with an increase in the continuum absorption in recent global climate models leading to an increase in shortwave absorption and better agreement with observations (e.g., Wild, 2020 and references therein). Using the Community Earth System Model, Kim et al. (2022) showed that an increase in shortwave absorption by water vapour could lead to a reduction in the global-mean rainfall. However, it should be noted that Kim et al. (2022) did not directly associate this increase in water vapour absorption to the continuum.

Most radiative transfer codes used in climate models parameterise water vapour continuum by the semi-empirical MT\_CKD (Mlawer-Tobin-Clough-Kneizys-Davies) model (Mlawer et al., 2012, 2023). Different versions of the MT\_CKD model are used in climate models with little or no justification even though the strengths of the water vapour continuum in these versions are significantly different in, especially, shortwave spectral regions. There are also significant disagreements between the strengths of the MT\_CKD model and other currently available water vapour continuum models (e.g., Elsey et al., 2020 and associated references). In fact, some recent studies have pointed out that the MT\_CKD model may be underestimating the strength of the water vapour continuum at some near-infrared atmospheric windows (e.g., Elsey et al., 2020). An increase in water vapour continuum absorption is expected to have more impact on the tropical atmosphere, since it has a higher water vapour content than the other atmospheres.

A few studies have investigated the effect of longwave water vapour continuum absorption on longwave radiative feedback (e.g., Koll et al., 2023; Roemer et al., 2024). However, equivalent studies in the shortwave have not been reported in the literature. This is clearly an oversight since the contribution of shortwave water vapour continuum absorption to radiative feedback in a warming climate is non-negligible (e.g., Jeevanjee, 2023). This paper presents an investigation on the impact of the uncertainty in the representation of the shortwave water vapour continuum on the clear-sky calculations of shortwave radiative feedback using a 1D RCE model. The radiative transfer calculations of this RCE model were performed using the fast and accurate European Centre for Medium-Range Weather Forecasts (ECMWF) radiation scheme (Hogan and Bozzo, 2018). The correlated  $k$ -distribution gas-optics tables for



the radiative transfer calculations were each trained with the water vapour continuum models selected for this work. These gas-optics tables were generated using the software tool developed recently by Hogan and Matricardi (2022). The rest of this paper is structured as follows: Section 2 will focus on the data and methods. In Section 3, the results from this work will be presented. Section 4 summarises and concludes.

## 2. Data and methodology

### 2.1. Water vapour continuum formulation

Four publicly available water vapour continuum models were selected for this study:

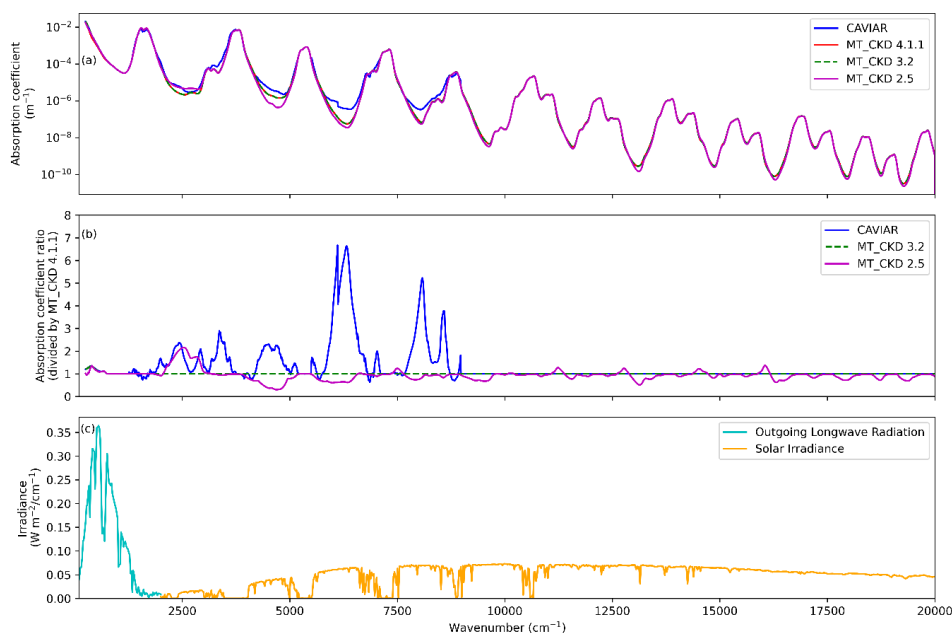
- CAVIAR (Continuum Absorption at Visible and Infrared Wavelengths and its Atmospheric Relevance) model (Ptashnik et al., 2011, 2012): This model was derived from extrapolated higher temperature laboratory measurements, but the self-continuum coefficients used here are from a recent update by Jon Elsey and Keith Shine in 2020 (Keith Shine, 2023, personal communication).
- MT\_CKD 4.1.1 (Mlawer et al., 2012, 2023): This is the most recent version of the MT\_CKD continuum model at the time this work was done.
- MT\_CKD 3.2 (Mlawer et al., 2012): This version resulted from a major revision of previous version(s) of the MT\_CKD continuum model.
- MT\_CKD 2.5 (Mlawer et al., 2012): This is arguably the most widely used version of the MT\_CKD continuum model and is still used in some climate models today. For example, it is used by the UK Met Office Unified Global Atmosphere 7.0/7.1 model (Walters et al., 2019).

Note that the strengths of other publicly available water vapour models, such as the BPS-MTCKD model (version 2.0; Paynter and Ramaswamy, 2014), fall within the range of the models selected here and thus there was no added value including them in this study. Figure 1(a) shows the absorption coefficients of these continuum models from about 0 – 20,000 cm<sup>-1</sup> in the 920 m thick atmospheric layer between ~960 hPa and ~860 hPa for the median profile of the Correlated K-Distribution Model Intercomparison Project datasets (CKDMIP; Hogan and Matricardi, 2020) while Figure 1(b) shows the absorption coefficient ratio of the other continuum models with that of MT\_CKD 4.1.1 model. The CAVIAR model is generally stronger than the other models (Figure 1(a)) in most atmospheric windows and some bands. Figure 1(b) shows that the CAVIAR model is much stronger than the MT\_CKD 4.1.1 model in near-infrared windows, where it is up to a factor of 7 stronger at the 6000 cm<sup>-1</sup> (1.6 μm)



135 window. The MT\_CKD 2.5 model is also stronger than the MT\_CKD 4.1.1 in the  $2500\text{ cm}^{-1}$  ( $5\text{ }\mu\text{m}$ ) window, but weaker in most regions of the shortwave. Between about  $250 - 700\text{ cm}^{-1}$ , the MT\_CKD 4.1.1 model is weaker than the other three models, except from about  $250 - 350\text{ cm}^{-1}$  where the MT\_CKD 2.5 model is weaker. The MT\_CKD 3.2 and MT\_CKD 4.1.1 models only differ in far-infrared region from  $250 - 700\text{ cm}^{-1}$ , where the MT\_CKD 3.2 is slightly stronger by a factor of up to about 1.3.

140 Figure 1(c) shows the terrestrial spectrum from  $0 - 2000\text{ cm}^{-1}$  and solar spectrum from  $2000 - 20000\text{ cm}^{-1}$  for a tropical atmosphere. Comparing these irradiances with the absorption coefficient ratios in Figure 1(b), it can be clearly seen that, in the shortwave, the continuum models differ most at near-infrared windows from about  $2500 - 10000\text{ cm}^{-1}$ .



145 **Figure 1. (a) Atmospheric absorption coefficients of CAVIAR (blue), MT\_CKD 4.1.1 (red), MT\_CKD 3.2 (green) and MT\_CKD 2.5 (purple) continuum models from  $0 - 20,000\text{ cm}^{-1}$ . (b) Absorption coefficient ratios of the other continuum models with that of the MT\_CKD 4.1.1 model. These absorption coefficients are for the 920 m thick atmospheric layer between  $\sim 960\text{ hPa}$  and  $\sim 860\text{ hPa}$  with temperatures about  $289\text{ K}$  and  $286\text{ K}$  and water vapour mole fraction about  $0.0137$  and  $0.0101$  and for the median profile of the CKDMIP datasets. The absorption coefficients were calculated by simply dividing layer optical depths of the CKDMIP median profile by the layer thickness of  $920\text{ m}$  calculated with the Hypsometric equation. (c) Low resolutions outgoing longwave radiation from**

150



the Earth's surface (cyan) and solar irradiance at ~960 hPa (orange). These irradiances  
 155 were calculated for a tropical atmosphere using the Atmospheric Radiative Transfer  
 Simulator (ARTS; Buehler et al., 2018, 2024).

## 2.2. Generation of correlated $k$ -distribution gas-optics tables

160 As stated in Section 1, the selected water vapour continuum models were parameterised in  $k$ -  
 distribution gas-optics tables (or models) required for radiative transfer calculations in the RCE  
 model.

Recently, Hogan and Matricardi (2022) developed a flexible and efficient software tool  
 ('ecCKD') that can be used to generate accurate correlated  $k$ -distribution gas-optics models for  
 165 radiation schemes of atmospheric models. These ecCKD gas-optics tables with fewer  $k$ -terms  
 ( $g$ -points) than other models, such as the widely used Rapid Radiative Transfer Model for  
 GCMs (RRTMG; Mlawer et al., 1997) gas-optics models, were shown to be very accurate  
 under clear-sky conditions by validating them against line-by-line (LBL) radiative transfer  
 calculations on independent data (Hogan and Matricardi, 2022). The flexibility of ecCKD  
 170 software tool allows the use of alternative water vapour continuum models for the training of  
 $k$ -distribution gas-optics tables. This flexibility was exploited to generate the gas-optics tables  
 used for this work.

The CKDMIP datasets, each consisting of spectral layer optical depths of 9 individual  
 gases ( $\text{H}_2\text{O}$ ,  $\text{O}_3$ ,  $\text{O}_2$ ,  $\text{N}_2$ ,  $\text{CO}_2$ ,  $\text{CH}_4$ ,  $\text{N}_2\text{O}$ , CFC-11 and CFC-12) in both the longwave (0 – 3260  
 175  $\text{cm}^{-1}$ ) and shortwave (250 – 50, 000  $\text{cm}^{-1}$ ), described by Hogan and Matricardi (2020) were  
 used. These optical depths were computed using the Line-By-Line Radiative Transfer Model  
 (LBLRTM; Clough et al., 2005), version 12.8, which incorporates MT\_CKD 3.2 water vapour  
 continuum (and continua of other gases). The datasets used here are made up of 64 profiles for  
 generating ecCKD gas-optics models and 50 profiles for independent evaluation.

180 To quantify the uncertainties in the water vapour continuum absorption on the gas-  
 optics tables produced using these datasets, Hogan and Matricardi (2020) produced an  
 additional set of water vapour profiles without the continuum. The continuum models selected  
 for this work were added to these water vapour continuum-free profiles in turn and used  
 together with the profiles of the other gases to generate the gas-optics tables. Four ecCKD gas-

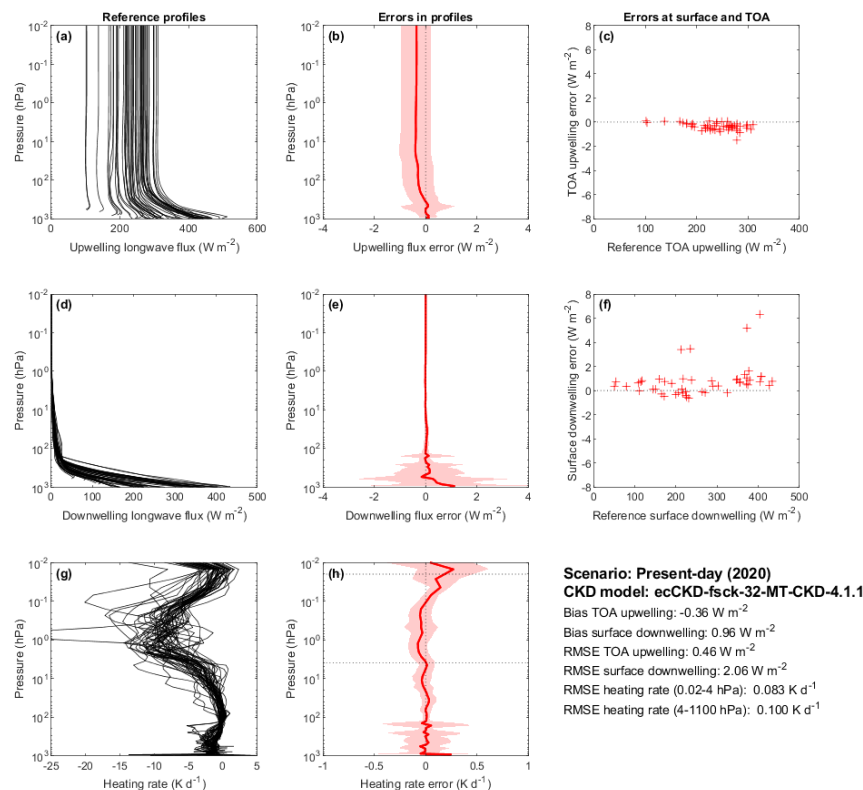


185 optics tables, trained by each of the 4 water vapour continuum models described in Section 2.1,  
were generated as described in Hogan and Matricardi (2022) and Hogan (2022).

These gas-optics tables were generated for climate applications, as this is the focus of  
this work (see Table 1, Hogan and Matricardi (2020)). The concentrations of gases and  
emission scenarios shown in Table 2 of Hogan and Matricardi (2020) were used. The following  
190 band structure were used: the RGB (red, green, blue) band structure with a heating-rate  
tolerance of  $0.047 \text{ K d}^{-1}$  for the shortwave and FSCK (full-spectrum correlated- $k$ ) band  
structure with a heating-rate tolerance of  $0.0161 \text{ K d}^{-1}$  for the longwave. These specifications  
resulted gas-optics models with 32  $k$ -terms in the shortwave and 32 to 34  $k$ -terms in the  
longwave. See Hogan and Matricardi (2022) and Hogan (2022) for details of these  
195 specifications.

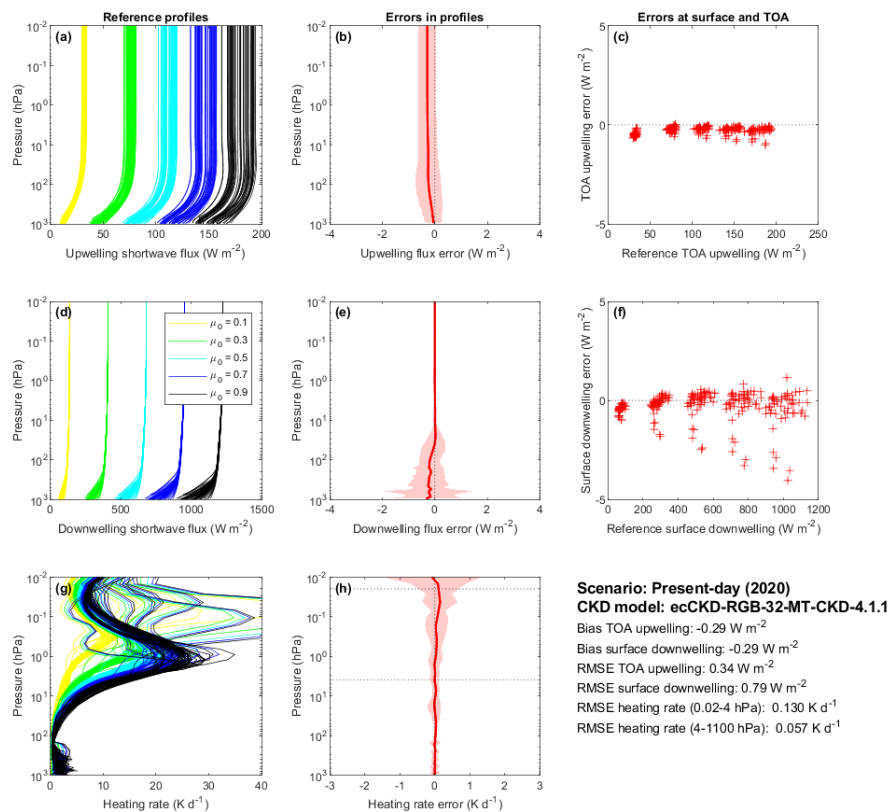
The generated gas-optics models were evaluated using LBL fluxes calculated from  
them (as described in Hogan, 2022) and LBL fluxes from the 50 profiles independent dataset.  
Figures 2 and 3 show, respectively, the evaluation of the longwave and shortwave gas-optics  
models both trained with MT\_CKD 4.1.1 for present-day concentrations of the well mixed  
200 greenhouse gases. Note that although we generated perturbed versions of both the longwave  
and shortwave gas-optics tables, only the shortwave perturbed gas-optics tables were actually  
used.

Figure 2 shows that the errors in the longwave fluxes do not exceed  $2 \text{ W m}^{-2}$  from the  
surface to the top-of-the-atmosphere while the root-mean-square error in the heating rates from  
205 the surface to the upper stratosphere (4 hPa) is only about  $0.10 \text{ K d}^{-1}$ .



**Figure 2: An evaluation of clear-sky longwave fluxes and heating rates from an ecCKD gas-optics table trained with the MT\_CKD 4.1.1 continuum model for the 50 independent profiles of the CKDMIP evaluation data set with present-day concentrations of greenhouse gases. Upwelling fluxes, downwelling fluxes and heating rates from the reference line-by-line calculations are shown in panels (a, d, g), while panels (b, e, h) show the corresponding biases in the calculations using the generated ecCKD gas-optics table. 95 % of the errors are within the shaded areas. Panels (c and f) depict instantaneous errors in upwelling top-of-atmosphere and downwelling surface fluxes. The statistics of the comparison are summarized in the bottom right panel.**





220 **Figure 3: As in Figure 2 but for the shortwave. The reference line-by-line calculations in panels (a, d, g) are for all 50 CKDMIP evaluation profiles at five values of the cosine of the solar zenith angle,  $\mu_0$  (0.1, 0.3, 0.5, 0.7, and 0.9). This gives a total of 250 combinations that are used in the subsequent evaluation.**

225 For the shortwave, the errors in the fluxes are about  $1 \text{ W m}^{-2}$  or less at all vertical levels as Figure 3 shows. This figure also shows that the heating rates errors are small, with the root-mean-square error in the heating rates from the surface to the upper stratosphere being only about  $0.057 \text{ K d}^{-1}$ .

230 For the gas-optics tables trained with the other three water vapour continuum models (MT\_CKD 2.5, MT\_CKD 3.2 and CAVIAR), both the shortwave and longwave errors in the upwelling fluxes, downwelling fluxes and heating rates are also small.



### 235 2.3. Radiation scheme

The Python code konrad (Dacie et al., 2019; Kluft et al., 2019) was used to construct the moist adiabatic atmosphere for the different surface temperatures (see Section 2.4) and to call the radiation scheme.

240 The default code for radiative transfer calculations in konrad is the Rapid Radiative Transfer Model for GCMs (RRTMG), a radiation scheme that is widely used in global and regional climate models (e.g., Pincus et al., 2015).

However, for this study, the offline version of the European Centre for Medium-Range Weather Forecasts (ECMWF) radiation scheme ('ecRad'; Hogan and Bozzo, 2018) was used in konrad through Python subprocesses. ecRad is an efficient, flexible, and fast radiation  
 245 scheme that is currently used in ECMWF Integrated Forecast System (IFS) and other models such as ICON (Icosahedral Nonhydrostatic) of the German Weather Service. Five solvers, including a 'cloudless' solver, are currently available in ecRad. The flexibility of this radiation scheme, which is based on its modular structure, enables it to be adapted for different uses. This flexibility was exploited to use any of the generated gas-optics models during each konrad  
 250 run. Also, since the focus of this study is on clear-sky conditions, radiative transfer calculations were performed using the 'cloudless' solver of ecRad.

### 2.4. Model configuration and calculations

Unless otherwise specified, all the calculations carried out in this study use the following  
 255 configuration of konrad.

The atmosphere was constructed on 512 levels of temperature and water vapour volume mixing ratio between 1000 and 0.01 hPa with no diurnal cycle. As recommended by the Radiative Convective Equilibrium Model Intercomparison Project (RCEMIP; Wing et al., 2018), the solar constant was set to  $551.58 \text{ W m}^{-2}$  and the zenith angle to  $42.05^\circ$ , resulting in  
 260 an insolation of  $409.6 \text{ W m}^{-2}$ . The surface in the model has a fixed surface temperature with prescribed values from 270 to 330 K (in 1 K increments) and an albedo is 0.2. Atmospheric temperature was set to follow a moist adiabat in the troposphere with the tropopause temperature fixed at 175 K. This moist adiabatic temperature profile is consistent with the assumption of RCE (e.g. Jeevanjee, 2023). Since the stratosphere is more in radiative  
 265 equilibrium rather than RCE, it was represented as an isothermal layer with this fixed tropopause temperature. This restriction also eliminates any stratospheric feedbacks. This is



the same setup as in, for example, Kluft et al. (2021), Jeevanjee (2023) and Roemer et al. (2024).

The relative humidity (RH) was set at a constant value of 80 % throughout the troposphere up to the cold-point tropopause. For the tropics, this value is higher than the observed average value of about 40 % from the mid to upper troposphere (e.g., Bourdin et al., 2021), but it was chosen to ensure that the amount of humidity in the upper levels of the troposphere is adequate for the interaction of lapse-rate and water-vapour feedbacks (Kluft et al., 2021). In the stratosphere, the specific humidity is kept constant at the value obtained at the cold-point tropopause. The concentrations of the other trace gases used are those specified by Kluft et al. (2019), including a CO<sub>2</sub> concentration of 348 ppmv and the ozone concentration profile defined according to RCEMIP guidelines.

The shortwave climate feedback parameter ( $\lambda_{sw}$ ) was calculated using the fixed-temperature method (Kluft et al., 2021) at a constant CO<sub>2</sub> concentration of 348 ppmv and surface temperature,  $T_s$ , from:

$$\lambda_{sw} = \frac{\Delta R(T_s + \Delta T) - \Delta R(T_s - \Delta T)}{2\Delta T}, \quad (1)$$

where  $\Delta R$  is the net shortwave radiation at the top of the atmosphere and  $\Delta T = 1$  K. Kluft et al. (2021) have justified the use of this fixed-temperature method by proving that results from it are in a very good agreement with those from the more frequently used linear regression method of Gregory et al. (2004) and have the advantage of being numerically more stable. For each  $T_s$ , we adjusted the tropospheric temperature ( $T$ ) and water vapour mixing ratio ( $q$ ) to the moist adiabat and calculated the clear-sky shortwave radiation. We then calculated  $\lambda_{sw}$  from Equation (1). This process is summarised in this simple flow chart:  $T_s \rightarrow$  tropospheric  $T$  and  $q$  profiles RCE adjustment  $\rightarrow$  shortwave radiation  $\rightarrow$  calculate  $\lambda_{sw}$ .

### 3. Results and discussion

For the atmospheric configuration described in Section 2.4, experiments were carried out in which the gas-optics table trained with the MT\_CKD 2.5, MT\_CKD 3.2 and CAVIAR continuum models was alternatively used for the shortwave radiation. The effect of the shortwave water vapour continuum uncertainty on the estimation of radiative feedback was obtained by comparing results from experiments in which MT\_CKD 2.5, MT\_CKD 3.2 and



CAVIAR models were used with those from an experiment in which the MT\_CKD 4.1.1  
 300 trained gas-optics table was used.

### 3.1 Radiative feedbacks for present-day surface temperature.

#### 3.1.1 Longwave feedback

For the clear-sky RCE framework adopted in this study, the longwave radiative feedback  
 305 parameter,  $\lambda_{\text{LW}}$ , could also be calculated using Equation 1. In this case,  $\Delta R$  is the net longwave  
 radiation at the top of the atmosphere. We remark here that the longwave feedback is not the  
 focus of this paper but was calculated for comparison with previous estimates.

For the MT\_CKD 4.1.1 model, the estimated clear-sky longwave feedback parameter  
 at 288 K surface temperature from this work,  $\lambda_{\text{LW}} \approx -1.864 \text{ W m}^{-2} \text{ K}^{-1}$ , agrees fairly well with  
 310 the values of  $\lambda_{\text{LW}}$  obtained from similar 1D studies for present-day average surface  
 temperatures. For example, at 288 K surface temperature, Xu and Koll (2024), Koll et al. (2023)  
 and Kluft et al. (2021) obtained values of about  $-1.9 \text{ W m}^{-2} \text{ K}^{-1}$ ,  $-2.0 \text{ W m}^{-2} \text{ K}^{-1}$  and  $-1.8 \text{ W m}^{-2}$   
 $\text{K}^{-1}$ , respectively for the clear-sky longwave feedback parameter.

#### 3.1.2 Shortwave feedback

At  $T_{\text{S}} = 288 \text{ K}$ , the clear-sky shortwave climate feedback parameters ( $\lambda_{\text{SW}}$ ) calculated are;  $0.364$   
 $\text{W m}^{-2} \text{ K}^{-1}$ ,  $0.365 \text{ W m}^{-2} \text{ K}^{-1}$ , and  $0.371 \text{ W m}^{-2} \text{ K}^{-1}$  for MT\_CKD 2.5, MT\_CKD 3.2 and  
 CAVIAR continuum models respectively. For the reference experiment, with the MT\_CKD  
 4.1.1 trained gas-optics table,  $\lambda_{\text{SW}} = 0.365 \text{ W m}^{-2} \text{ K}^{-1}$ . If needed, the total radiative feedback  
 320 parameter for each continuum model from this study can be readily obtained by using the  
 additive property of feedbacks; total feedback,  $\lambda_{\text{tot}} = \lambda_{\text{LW}} + \lambda_{\text{SW}}$ , where  $\lambda_{\text{LW}}$  is given in Section  
 3.1.1.

Under clear-sky conditions, the shortwave feedback is due mainly to the absorption of  
 solar radiation by water vapour. Since the amount of atmospheric water vapour depends on  
 325 temperature, shortwave absorption by water vapour gives an extra positive feedback in climate  
 change. This is because in a warmer world, the amount of water vapour in the atmosphere  
 increases (scaling with the Clausius-Clapeyron relation for a fixed RH). This leads to more  
 absorption of solar radiation, which is a positive feedback. A stronger shortwave continuum  
 means a further increase in absorbed solar radiation in a warming world leading to a stronger  
 330 positive shortwave feedback. Thus, the shortwave radiative feedback tends to be more positive



with increasing strength of the shortwave water vapour continuum as the values of  $\lambda_{\text{sw}}$  given above show.

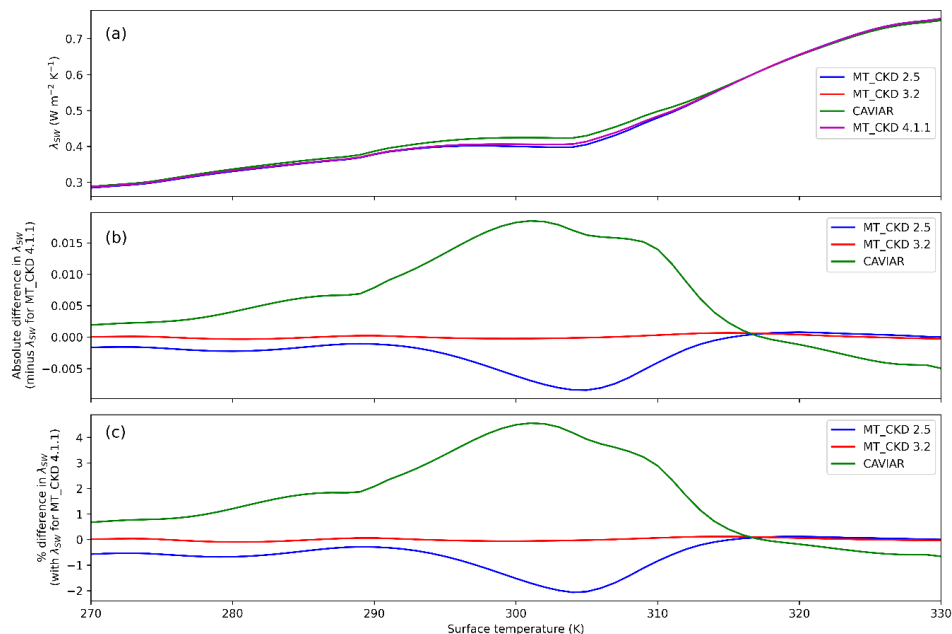
The values of  $\lambda_{\text{sw}}$  obtained here show that compared to MT\_CKD 4.1.1, differences in shortwave MT\_CKD models make a negligible contribution to the estimated shortwave radiative feedback. The shortwave feedback using the weaker MT\_CKD 2.5 model is only  
 335 about  $0.001 \text{ W m}^{-2} \text{ K}^{-1}$  ( $\sim 0.3 \%$ ) less positive than that with MT\_CKD 4.1.1. The feedbacks with MT\_CKD 3.2 and 4.1.1 models are equal, which is expected, since their strengths in the shortwave are equal as discussed in Section 2.1. However, relative to MT\_CKD 4.1.1, the stronger CAVIAR shortwave continuum model increases the shortwave feedback by about  
 340  $0.006 \text{ W m}^{-2} \text{ K}^{-1}$  ( $\sim 1.6 \%$ ).

Thus, if the shortwave water vapour continuum absorption is as strong as suggested by the CAVIAR model, then there may be a slight underestimation of clear-sky shortwave radiative feedback from 1D RCE models with the MT\_CKD continuum model for present-day surface temperature of 288 K.

345

### 3.2. Temperature-dependence of the shortwave radiative feedback

As discussed in Section 3.1.2, the shortwave radiative feedback depends quite strongly on the surface temperature,  $T_s$  because there is more moisture in a warmer atmosphere. In this section, the impact of changing  $T_s$  on  $\lambda_{\text{sw}}$  will be presented. As a function of  $T_s$ , Figure 4 (a) shows the  
 350 variation of  $\lambda_{\text{sw}}$  for all four continuum models considered in this study, while Figure 4 (b and c) show respectively, the absolute and percentage continuum induced error in  $\lambda_{\text{sw}}$  (with respect to calculations using MT\_CKD 4.1.1). Figure 4(a) shows that  $\lambda_{\text{sw}}$  increases with  $T_s$  for all continuum models (from slightly less than  $0.300 \text{ W m}^{-2} \text{ K}^{-1}$  at 270 K to slightly above  $0.750 \text{ W m}^{-2} \text{ K}^{-1}$  at 330 K). Increased atmospheric moisture at higher temperatures reduces the  
 355 upwelling shortwave radiation leading to an increase in the net shortwave radiation at the top of the atmosphere and hence  $\lambda_{\text{sw}}$ . This figure shows that the  $\lambda_{\text{sw}}$  due to the use of CAVIAR model is not always greater than the  $\lambda_{\text{sw}}$  estimated using the other models at all surface temperature as hinted by calculations at  $T_s = 288 \text{ K}$ .



360 **Figure 4.** As a function of surface temperature ( $T_s$ ), (a) variation of clear-sky shortwave climate feedback parameter ( $\lambda_{sw}$ ) estimated using the MT\_CKD 2.5 (blue), MT\_CKD 3.2 (red), CAVIAR (green) and the chosen reference MT\_CKD 4.1.1 (magenta) continuum models; (b) absolute difference in  $\lambda_{sw}$  (with respect to values calculated using MT\_CKD 4.1.1 model); (c) percent differences in  $\lambda_{sw}$  (with respect to calculations using MT\_CKD 4.1.1).

Figure 4(b and c) show that the relative error in  $\lambda_{sw}$  that is induced by the continuum uncertainty also depends relatively strongly on the surface temperature. Compared to shortwave feedback calculated with the MT\_CKD 4.1.1 model, the shortwave feedback with the MT\_CKD 2.5 model is up to  $\sim 0.008 \text{ W m}^{-2} \text{ K}^{-1}$  ( $\sim 2.0 \%$ ) less at a surface temperature of  $\sim 305 \text{ K}$ . From  $T_s$  of about  $305 - 315 \text{ K}$ , the relative error in estimated shortwave feedbacks due to differences in the strength between these two continuum models is less than this value. For  $T_s$  greater than  $\sim 318 \text{ K}$ , the shortwave feedbacks with both models are equal and the uncertainty in  $\lambda_{sw}$  due to these continuum models is zero. This figure also shows that the uncertainty in estimated shortwave feedbacks due to the differences between the MT\_CKD 3.2 and MT\_CKD 4.1.1 models is zero (as expected) and show virtually no temperature dependence.



The estimated shortwave feedback with the CAVIAR model is up to  $\sim 0.018 \text{ W m}^{-2} \text{ K}^{-1}$  ( $\sim 4.6 \%$ ) more positive than that with the MT\_CKD 4.1.1 model at a surface temperature of  $\sim 301 \text{ K}$  as Figure 4 (b and c) shows. From  $T_s$  of about  $301 - 316 \text{ K}$ , this relative error decreases with surface temperature. Beyond  $T_s$  of about  $316 \text{ K}$ , the feedback with CAVIAR model is less positive than that with MT\_CKD 4.1.1 model and increases negatively with temperature (but only up to about  $0.005 \text{ W m}^{-2} \text{ K}^{-1}$  or  $\sim 0.7 \%$  less).

The way the continuum induced uncertainty in  $\lambda_{\text{SW}}$  changes with surface temperature (Figure 4(b and c)) can presumably be explained by spectral variations in both the water vapour spectroscopy and in the differences between the CAVIAR and MT\_CKD models. Shortwave water vapour absorption generally tends to decrease with increasing wavenumber (Figure 1(a)). At the same time, the largest discrepancies between CAVIAR and MT\_CKD occur at intermediate wavenumbers within the near-infrared, that is, in the atmospheric windows around  $4000 \text{ cm}^{-1}$ ,  $6000 \text{ cm}^{-1}$ , and  $8000 \text{ cm}^{-1}$ , respectively. This is relevant because, broadly speaking,  $\lambda_{\text{SW}}$  presumably originates at wavenumbers at which the transmissivity of the atmosphere changes most rapidly, that is, at column-integrated opacities of order unity ( $\tau_{\text{col}} \approx 1$ ). At low  $T_s$  – and thus low water vapour concentration –  $\tau_{\text{col}} \approx 1$  primarily occurs within the strong absorption bands below  $4000 \text{ cm}^{-1}$ , where CAVIAR and MT\_CKD are not very different and thus the difference in  $\lambda_{\text{SW}}$  is small. As  $T_s$  – and thus water vapour concentration – increases,  $\tau_{\text{col}} \approx 1$  more frequently occurs in the above mentioned windows where CAVIAR and MT\_CKD differ substantially. Consequently, a large portion of  $\lambda_{\text{SW}}$  originates in these windows at  $T_s$  around  $300 \text{ K}$ , contributing to the substantial uncertainty there. At even higher  $T_s$ ,  $\tau_{\text{col}} \approx 1$  occurs at even higher wavenumbers, where the differences between CAVIAR and MT\_CKD are small, and thus the uncertainty in  $\lambda_{\text{SW}}$  is also small. We remark that this small error in  $\lambda_{\text{SW}}$  due to the small differences between the CAVIAR and MT\_CKD at wavenumbers higher than  $\sim 8000 \text{ cm}^{-1}$  may be simply because water vapour continuum has not been successfully measured at these wavenumbers (it has only been extrapolated based on measurements from shorter wavenumbers). The lack of complete understanding of the water vapour continuum at these high wavenumbers may also be responsible for its absorption having little or no impact on estimated  $\lambda_{\text{SW}}$  at  $T_s$  above about  $316 \text{ K}$  (Figure 4(b and c)).

The shortwave feedbacks calculated here at temperatures above  $\sim 296 \text{ K}$  are subjected to two uncertainties. Firstly, the temperature dependence of the water vapour self-continuum in ecRad is fitted at  $260$  and  $296 \text{ K}$ . This increases the error in the self-continuum and hence estimated feedbacks for surface temperatures above  $\sim 296 \text{ K}$ . Secondly, a reduction in the



validity of some assumptions of the 1D-RCE framework at temperatures greater than 310 K adds to the uncertainties in calculated feedbacks (Kluft et al., 2021).

#### 4. Summary and conclusions

415 Radiative transfer calculations for a moist adiabatic troposphere at different surface temperatures have been used to study the impact of the differences in the strength of the water vapour continuum in the shortwave spectral region on shortwave radiative feedback. Three versions of the semi-empirical MT\_CKD (2.5, 3.2 and 4.1.1) and the laboratory-implied CAVIAR water vapour continuum models were selected for this work. This effect was studied  
 420 through radiative transfer calculations using shortwave correlated- $k$  gas-optics tables trained with different continuum models. The ECMWF fast and accurate radiation scheme was used for the radiative transfer calculations. The atmosphere had a fixed RH of 80 %, a moist adiabatic temperature profile in the troposphere and fixed surface temperature between 270 and 330 K. The stratosphere was considered as an isothermal layer with the tropopause temperature  
 425 fixed at 175 K.

For present-day average surface temperature of 288 K, an increase in the strength of the shortwave water vapour continuum led to a more positive shortwave feedback. At this temperature, the discrepancies in the strength of the shortwave water vapour continuum lead to very small uncertainties in the estimated shortwave radiative feedback between the three  
 430 MT\_CKD models; only up to about  $0.001 \text{ W m}^{-2} \text{ K}^{-1}$  ( $\sim 0.3 \%$ ). However, compared to calculations with the MT\_CKD 4.1.1 model, the shortwave feedback due to the use of the stronger CAVIAR continuum is about  $0.006 \text{ W m}^{-2} \text{ K}^{-1}$  ( $\sim 1.6 \%$ ) more positive.

The estimated shortwave radiative feedbacks depends relatively strongly on the surface temperature. The relative error in shortwave feedbacks due to changes in the MT\_CKD  
 435 continuum models increases with surface temperature to a maximum of  $\sim 0.008 \text{ W m}^{-2} \text{ K}^{-1}$  ( $\sim 2.0 \%$ ) at  $T_s \approx 305 \text{ K}$ . When the CAVIAR continuum model was used, the shortwave feedback uncertainty increases with surface temperature to a maximum of  $\sim 0.018 \text{ W m}^{-2} \text{ K}^{-1}$  ( $\sim 4.6 \%$ ) at  $T_s \approx 300 \text{ K}$ , when compared with that estimated using MT\_CKD 4.1.1. The continuum induced error in  $\lambda_{\text{SW}}$  is small at low  $T_s$  (close to 270 K) and at high  $T_s$  (above  $\sim 300 \text{ K}$ ) because of the  
 440 spectral variations in both the water vapour spectroscopy and in the differences between the CAVIAR and MT\_CKD models.

The results from this study show that a revision of the MT\_CKD water vapour continuum model in the shortwave over the past decade has a small and negligible effect on the clear-sky shortwave radiative feedback computed from a 1D RCE model for present-day





445 average surface temperature. Compared to the MT\_CKD 4.1.1 model, the stronger CAVIAR  
water vapour continuum model has a relatively greater impact on the shortwave radiative  
feedback at a surface temperature of about 288 K. For higher surface temperatures, the impact  
of uncertainties of water vapour continuum on the estimation of shortwave feedbacks is higher.  
Thus, using the MT\_CKD model in RCE models may lead to an underestimation of the  
450 shortwave feedback, if it is underestimating the strength of the shortwave water vapour  
continuum as some studies suggest. It is therefore important for the water vapour continuum in  
the shortwave to be constrained, as this will contribute to reducing the discrepancies in the  
estimation of shortwave radiative feedback, especially in a warming world.

It has been hypothesised that thin clouds in the atmosphere create a longer pathlength  
455 for solar radiation and can thus enhance water vapour continuum absorption at transparency  
windows in the shortwave. In a future study, we plan to study the impact of this enhanced  
absorption on radiative feedback.

#### 460 **Author contributions**

KM and SB conceptualized and designed the experiments, and KM carried them out. LK and  
FR contributed to the development of the model code. RH and KM generated the gas-optics  
tables for the radiative transfer calculations. KM prepared the manuscript with input from all  
co-authors.

465

#### **Acknowledgments**

This study contributes to the Cluster of Excellence “CLICCS — Climate, Climatic Change,  
and Society”, and to the Center for Earth System Research and Sustainability (CEN) of  
University of Hamburg. The authors thank Matthew Chandry and Oliver Lemke for their  
470 assistance in coupling ecRad to konrad. Manfred Brath is acknowledged for his assistance in  
simulating the terrestrial and solar spectrum shown in Figure 1. Kaah P. Menang was sponsored  
by the Alexander von Humboldt foundation under the program ‘Humboldt Research  
Fellowship Programme for Experienced Researchers’.

#### 475 **Conflict of interest**

The authors declare that they have no conflict of interest.



## References

- Buehler, S. A., Larsson, R., Lemke, O., Pfreundschuh, S., Brath, M., Adams, I., Fox, S.,  
 480 Roemer, F., Czarnecki, P., and Eriksson, P.: The Atmospheric Radiative Transfer Simulator  
 ARTS, Version 2.6 - Deep Python Integration, *J. Quant. Spectrosc. Radiat. Transfer*, 2024  
 (submitted), <http://ssrn.com/abstract=4815661>, draft available at <https://arts.mi.uni-hamburg.de/publications/group.php>.
- 485 Buehler, S. A., Mendrok, J., Eriksson, P., Perrin, A., Larsson, R., And Lemke, O.: ARTS, the  
 Atmospheric Radiative Transfer Simulator - Version 2.2, the planetary toolbox edition, *Geosci.  
 Model Dev.*, 11: 1537-1556, doi: 10.5194/gmd-11-1537-2018, 2018.
- Bourdin, S., Kluft, L., and Stevens, B.: Dependence of climate sensitivity on the given  
 490 distribution of relative humidity, *Geophys. Res. Lett.*, 48, e2021GL092462, doi:  
 10.1029/2021GL092462, 2021.
- Clough, S. A., Shephard, M. W., Mlawer, E. J., Delamere, J. S., Iacono, M. J., Cady-Pereira,  
 K., Boukabara, S., and Brown, P. D.: Atmospheric radiative transfer modeling: a summary of  
 495 the AER codes, *J. Quant. Spectrosc. Radiat. Transf.*, 91: 233–244, doi:  
 10.1016/j.jqsrt.2004.05.058, 2005.
- Dacie, S., Kluft, L., Schmidt, H., Stevens, B., Buehler, S. A., Nowack, P. J., Dietmüller, S.,  
 Abraham, N. L., and Birner, T.: A 1D RCE study of factors affecting the tropical tropopause  
 500 layer and surface climate. *J. Climate*, 32: 6769-6782, doi: 10.1175/JCLI-D-18-0778.1, 2019.
- Else, J., Coleman, M. D., Gardiner, T. D., Menang, K. P., and Shine, K. P.: Atmospheric  
 observations of the water vapour continuum in the near-infrared windows between 2500 and  
 6600 cm<sup>-1</sup>, *Atmos. Meas. Tech.*, 13: 2335-2361, doi:10.5194/amt-13-2335-2020, 2020.  
 505
- Gregory, J. M., Ingram, W. J., Palmer, M. A., Jones, G. S., Stott, P. A., Thorpe, R. B., and  
 Williams, K. D.: A new method for diagnosing radiative forcing and climate sensitivity,  
*Geophys. Res. Lett.*, 31(3): 1–4, doi:10.1029/2003GL018747, 2004.
- 510 Hogan, R. J.: The ECMWF Correlated K-Distribution Tool (ecCKD): User Guide (v1.1), 2022.



Hogan, R. J., and Bozzo, A.: A flexible and efficient radiation scheme for the ECMWF model, *J. Adv. Model. Earth Syst.*, 10, 1990–2008, doi: 10.1029/2018MS001364, 2018.

515 Hogan, R. J., and Matricardi, M.: Evaluating and improving the treatment of gases in radiation schemes: The Correlated K-Distribution Model Intercomparison Project (CKDMIP), *Geosci. Model Dev.*, 13(12), 6501–6521, doi: 10.5194/gmd-13-6501-2020, 2020.

Hogan, R. J., and Matricardi, M.: A tool for generating fast *k*-distribution gas-optics models for  
 520 weather and climate applications, *J. Adv. Model. Earth Syst.*, 14, e2022MS003033, doi: 10.1029/2022MS003033, 2022.

Jeevanjee, N.: Climate sensitivity from radiative-convective equilibrium: A chalkboard approach, *Am. J. Phys.* 91, 731–745, doi: 10.1119/5.0135727, 2023.

525

Kim, H., Pendergrass, A. G. and Kang, S. M.: The dependence of mean climate state on shortwave absorption by water vapor, *J. Climate*, 35:2189–2207, doi: 10.1175/JCLI-D-21-0417.1, 2022.

530 Kluft, L.: *Benchmark calculation of the climate sensitivity of radiative-convective equilibrium*, PhD thesis, Universität Hamburg, Hamburg, Germany, doi:10.17617/2.3274272, 2020.

Kluft, L., Dacie, S., Brath, M., Buehler, S. A., and Stevens, B.: Temperature-dependence of the clear-sky feedback in radiative-convective equilibrium, *Geophys. Res. Lett.*, 48, e2021GL094649, doi: 10.1029/2021GL094649, 2021.  
 535

Kluft, L., Dacie, S., Buehler, S. A., Schmidt, H., and Stevens, B.: Re-examining the first climate models: Climate sensitivity of a modern radiative-convective equilibrium model, *J. Climate*, 32: 8111–8125, doi: 10.1175/JCLI-D-18-0774.1, 2019.

540

Koll, D. D. B., Jeevanjee, N., and Lutsko, N. J.: An Analytic Model for the Clear-Sky Longwave Feedback, *J. Atmos. Sci.*, 80: 1923–1951, doi: 10.1175/JAS-D-22-0178.1, 2023.



Kratz, D. P.: The sensitivity of radiative transfer calculations to changes in the HITRAN  
 545 database from 1982 to 2004, *J. Quant. Spectrosc. Radiat. Transf.*, 109: 1060-1080, doi:  
 10.1016/j.jqsrt.2007.10.010, 2008.

Manabe, S., and Wetherald, R. T.: Thermal equilibrium of the atmosphere with a given  
 distribution of relative humidity, *J. Atmos. Sci.*, 24: 241–259, doi:  
 550 10.1175/15200469(1967)024<0241:TEOTAW.2.0.CO;2, 1967.

Meraner, K., Mauritsen, T., and Voigt, A.: Robust increase in equilibrium climate sensitivity  
 under global warming, *Geophys. Res. Lett.*, 40: 5944-5948, doi: 10.1002/2013GL058118,  
 2013.

555

Mlawer, E. J., Cady-Pereira, K. E., Mascio, J., and Gordon, I. E.: The Inclusion of the  
 MT\_CKD Water Vapor Continuum Model in the HITRAN Molecular Spectroscopic Database,  
*J. Quant. Spectrosc. Radiat. Transf.*, 306: 108645, doi: 10.1016/j.jqsrt.2023.108645, 2023.

560 Mlawer, E. J., Payne, V. H., Moncet, J.-L., Delamere, J. S., Alvarado, M. J., and Tobin, D. C.:  
 Development and recent evaluation of the MT\_CKD model of continuum absorption, *Philos.*  
*T. Roy. Soc. A*, 370: 2520-2556, doi: 10.1098/rsta.2011.0295, 2012.

Mlawer, E. J., Taubman, S. J., Brown, P. D., Iacono, M. J., and Clough, S. A.: Radiative transfer  
 565 for inhomogeneous atmospheres: RRTM, a validated correlated-k model for the longwave, *J.*  
*Geophys. Res.*, 102: 16 663-16 682, doi: 10.1029/97JD00237, 1997.

Popke, D., Stevens, B., and Voigt, A.: Climate and climate change in a radiative-convective  
 equilibrium version of ECHAM6, *J. Adv. Model. Earth Syst.*, 5: 1-14, doi:  
 570 10.1029/2012MS000191, 2013.

Paynter, D., and Ramaswamy, V.: Investigating the impact of the water vapor continuum upon  
 climate simulations using GFDL global models, *J. Geophys. Res.-Atmos.*, 119: 10720-10737,  
 doi: 10.1002/2014JD021881, 2014.

575

Pincus, R., Mlawer, E. J., Oreopoulos, L., Ackerman, A. S., Baek, S., Brath, M., Buehler, S. A.,  
 Cady-Pereira, K. E., Cole, J. N. S., Dufresne, J.-L., Kelley, M., Li, J., Manners, J., Paynter, D.



- J., Roehrig, R., Sekiguchi, M., and Schwarzkopf, D. M.: Radiative flux and forcing parameterization error in aerosol-free clear skies, *Geophys. Res. Lett.*, 42: 5485-5492, doi: 10.1002/2015GL064291, 2015.
- 580 Ptashnik, I. V., McPheat, R. A., Shine, K. P., Smith, K. M., and Williams, R. G.: Water vapor self-continuum absorption in near-infrared windows derived from laboratory measurements, *J. Geophys. Res.* 116: D16305, doi: 10.1029/2011J D015603, 2011.
- 585 Ptashnik, I. V., McPheat, R. A., Shine, K. P., Smith, K. M., and Williams, R. G.: Water vapour foreign-continuum absorption in near-infrared windows from laboratory measurements, *Philos. Trans. Roy. Soc. A*, 370: 2557-2577, doi: 10.1098/rsta.2011.0218, 2012.
- Ramanathan, V., and Coakley, J. A.: Climate modeling through radiative-convective models, 590 *Rev. Geophys. Space Phys.*, 16: 465-489, doi: 10.1029/RG016i004p00465, 1978.
- Reed, K. A., Medeiros, B., Bacmeister, J. T., and Lauritzen, P. H.: Global radiative-convective equilibrium in the Community Atmosphere Model, version 5, *J. Atmos. Sci.*, 72: 2183-2197, doi:10.1175/JAS-D-14-0268.1, 2015.
- 595 Roemer, F. E., Buehler, S. A., Kluft, L., and Pincus, R.: Effect of Uncertainty in Water Vapor Continuum Absorption on CO<sub>2</sub> Forcing, Longwave Feedback, and Climate Sensitivity, *J. Adv. Model. Earth Syst.*, 16: e2023MS004157, doi: 10.1029/2023MS004157, 2024.
- 600 Schlesinger, M. E.: Equilibrium and transient climatic warming induced by increased atmospheric CO<sub>2</sub>, *Climate Dyn.*, 1: 35-51, doi: 10.1007/BF01277045, 1986.
- Shine, K. P., Campargue, A., Mondelain, D., McPheat, R. A., Ptashnik, I. V., and Weidmann, D.: The water vapour continuum in near infrared windows – Current understanding and 605 prospects for its inclusion in spectroscopic databases, *J. Mol. Spectrosc.*, 327: 193–208, doi: 10.1016/j.jms.2016.04.011, 2016.
- Xu, Y., and Koll, D. D. B.: CO<sub>2</sub>-dependence of longwave clear-sky feedback is sensitive to temperature, *Geophys. Res. Lett.*, 51: e2024GL108259, doi: 10.1029/2024GL108259, 2024.
- 610



- Walters, D., Baran, A. J., Boutle, I., Brooks, M., Earnshaw, P., Edwards, J., Furtado, K., Hill, P., Lock, A., Manners, J., Morcrette, C., Mulcahy, J., Sanchez, C., Smith, C., Stratton, R., Tennant, W., Tomassini, L., Van Weverberg, K., Vosper, S., Willett, M., Browse, J., Bushell, A., Carslaw, K., Dalvi, M., Essery, R., Gedney, N., Hardiman, S., Johnson, B., Johnson, C.,  
 615 Jones, A., Jones, C., Mann, G., Milton, S., Rumbold, H., Sellar, A., Ujiie, M., Whittall, M., Williams, K., and Zerroukat, M.: The Met Office Unified Model Global Atmosphere 7.0/7.1 and JULES Global Land 7.0 configurations, *Geosci. Model Dev.*, 12: 1909–1963, doi: 10.5194/gmd-12-1909-2019, 2019.
- 620 Wild, M.: The global energy balance as represented in CMIP6 climate models, *Climate Dyn.*, 55: 553–577, doi: 10.1007/s00382-020-05282-7, 2020.
- Wing, A. A., Reed, K. A., Satoh, M., Stevens, B., Bony, S., and Ohno, T.: Radiative-convective equilibrium model intercomparison project, *Geosci. Model Dev.*, 11, 793–813, doi:  
 625 10.5194/gmd-11-793-2018, 2018.
- Wing, A. A., Stauffer, C. L., Becker, T., Reed, K. A., Ahn, M.-S., Arnold, N. P., et al.: Clouds and convective self-aggregation in a multimodel ensemble of radiative-convective equilibrium simulations. *J. Adv. Model. Earth Syst.*, 12: e2020MS002138, doi: 10.1029/2020MS002138,  
 630 2020.